Computer simulation comparison of CCDs and APDs for curvature wavefront sensing

Thomas V. Craven-Bartle, Reinhold J. Dorn, James W. Beletic

European Southern Observatory, Munich
Karl Schwarzschild str. 2, D-85748 Garching bei München, Germany

ABSTRACT

In this paper, the results from a computer simulation comparison between curvature AO-systems using APDs and a special-purpose curvature-CCD, the MIT/LL CCID-35, are presented. The simulated AO-system is the MACAO 60-element curvature system[1], which is being developed by ESO for the Very Large Telescope (VLT) and VLT Interferometer (VLTI). The results indicate a difference in performance of 5% Strehl in K-band for a 15th magnitude guide star, 2% Strehl for a 16th magnitude star, and less than 0.6% Strehl for all other magnitude guide stars.

Keywords: Adaptive optics, curvature wavefront sensing, computer simulation, detectors, CCD, avalanche photo diode

1. INTRODUCTION

1.1 Background

At the European Southern Observatory (ESO), several adaptive optics systems using curvature wavefront sensors are being developed for the Very Large Telescope (VLT) and the VLT interferometer (VLTI). Curvature AO-systems have traditionally used avalanche photo diodes (APDs) as detectors. APDs are photon-counting devices that produce a pulse on their output whenever a photon is detected. The great advantage of APDs is that they have no read-out noise and that the read-out is almost instantaneous. However, they have some serious drawbacks compared to charge-coupled devices (CCDs):

- ***Small dynamic range***. For the duration of the avalanche of electrons – typically around 40 ns – the APD is blind to any new photons arriving. This limits the dynamic range of the APD and calls for the use of neutral density filters to adapt the incident photon flux to the dynamic range of the APD. CCDs, on the other hand, have an enormous dynamic range and thus require no filters.
- ***Low quantum efficiency***. The quantum efficiency, which is the probability that an incident photon is detected, is lower for APDs than for CCDs. APDs typically have a peak quantum efficiency of 70% at 700nm, while the same number for CCDs is over 90%.
- ***High dark current***. APDs generate *dark current*, or false photon counts, of 100 to 250 counts per second depending on the cost of the APDs, while a well-cooled CCD generates a negligible amount of dark current. The dark current affects the performance of the system when faint guide stars are used.
- ***High cost***. A 60-element AO-system using APDs is significantly more expensive than one using a CCD.

The drawbacks of the CCDs are their read-out delay and read-out noise.

The above facts combined with advances in CCD-technology motivated an investigation of the use of a special-purpose curvature-CCD as the wavefront sensor detector in a 60-element curvature AO system.

1.2 Method of comparison

A common measure used to quantify the performance of an AO-system is the *Strehl ratio*, or *Strehl* for short, of the corrected point spread function (PSF). The Strehl is defined as the ratio of the maximum intensity in the PSF to the maximum intensity in the diffraction-limited PSF of the instrument. Two types of Strehl-ratios can be measured: *instantaneous* Strehl (or *short-exposure* Strehl) and *integrated* Strehl (or *long-exposure* Strehl). The latter is of most interest to astronomers, since long exposure times are usually used.

To compare the performance of the two types of detectors, a computer model of the atmosphere, telescope and AO-system was developed in MatLab. Using the computer model, the Strehl ratio in K-band was measured for guide stars of magnitude 10 to 18 and compared for the different detectors.

2. PRINCIPLE OF THE CURVATURE-CCD

2.1 Introduction to curvature wavefront sensing

The curvature wavefront sensor measures the intensity I_1 in an intrafocal plane and the intensity I_2 in an extrafocal plane and compares these intensities to determine the curvature of the wavefront. As the normalised difference, $(I_1–I_2)/(I_1+I_2)$, is used for the comparison, and I_1 and I_2 are measured simultaneously, the sensor is not susceptible to the non-uniform illumination due to scintillation.

Two different detectors never have exactly the same characteristics. Using separate detectors to measure the intrafocal and extrafocal intensities and calculating the normalised difference will compare not only the intensities, but also the detectors themselves; differences in detector characteristics will generate false curvature signals. To avoid these problems, an oscillating membrane mirror is used to modulate the location of the plane being imaged on a single detector. During one half-cycle of the membrane motion, the detector records the intrafocal distribution of light, and during the other half-cycle it records the extrafocal distribution. As long as the membrane frequency is higher than the speed at which scintillation evolves, scintillation will not affect the curvature signal.

Before detection, the light passes through a lenslet array that integrates the light spatially and focuses it on optical fibers that lead it to the detectors. Fig. 1 shows a possible optical layout of an adaptive optics system based on curvature wavefront sensing.

2.2 The curvature-CCD

Ordinary CCDs are not well suited for use in curvature wavefront sensors. The reason is that the detector must be read out twice every membrane cycle in order to tell apart the photoelectrons collected during the intrafocal and extrafocal periods. With the membrane running at two kilohertz, a CCD with a frame-rate of four kilohertz would have to be used. At the current state of detector technology, the signal from the CCD would be dominated by read-out noise at this speed.

However, if the charge collected during the intrafocal period could be stored away on the chip during the extrafocal period, and vice versa, the CCD would only need to be read out when a new curvature signal is to be calculated. This is the principle of the *CCD for Curvature Wavefront Sensing*, which was first presented at the ESO CCD 1999 Workshop[2]. This chip shifts the extrafocal and intrafocal photoelectrons integrated in each super pixel between the sensor area and charge storage areas on either side of the super pixel. The CCD is then read out slowly while the next integration starts on the chip. Using this technique, a read-out noise of two electrons RMS with a read-out delay of 250 μs is expected. This has been verified at ESO in 1999 by Reinhold Dorn on a frontside MIT/LL CCID-20 at 100 kilopixels per second, which has the same output amplifier as the MIT/LL CCID-35. Fig. 2 shows the chip layout of the MIT/LL CCID-35.

As ESO has developed FIERA[3], a standard controller for CCDs, the substantial task of controlling the curvature-CCD can be considered solved.

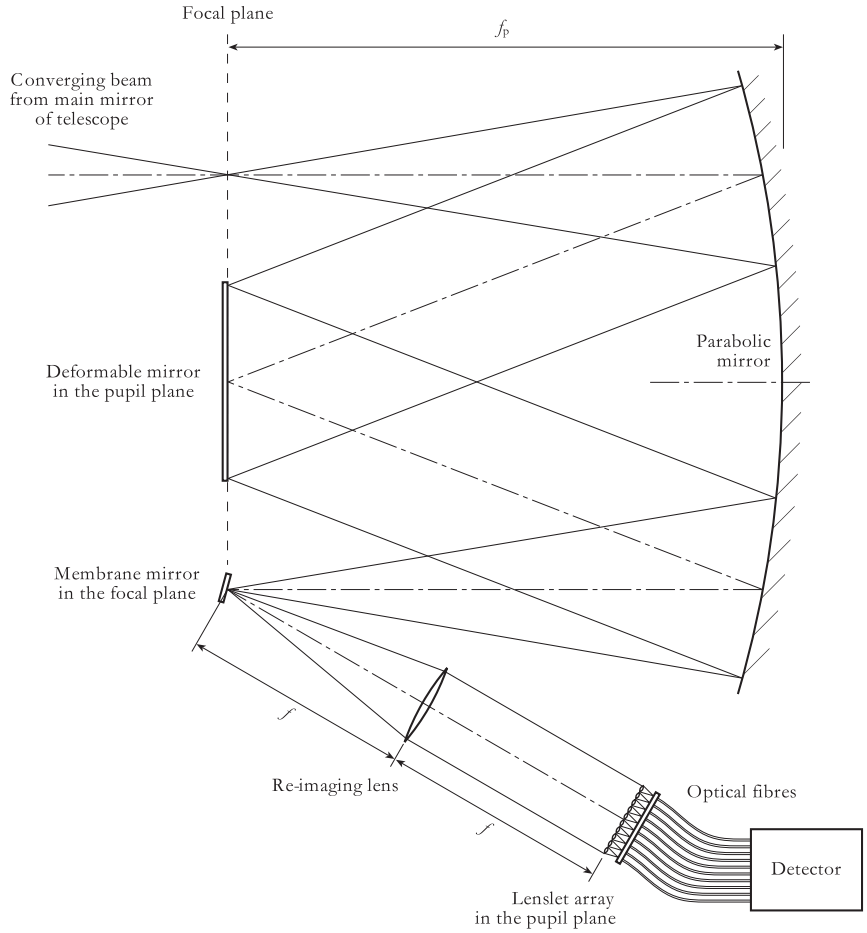

Fig. 1. Optical layout of a curvature wavefront sensor-based adaptive optics system.

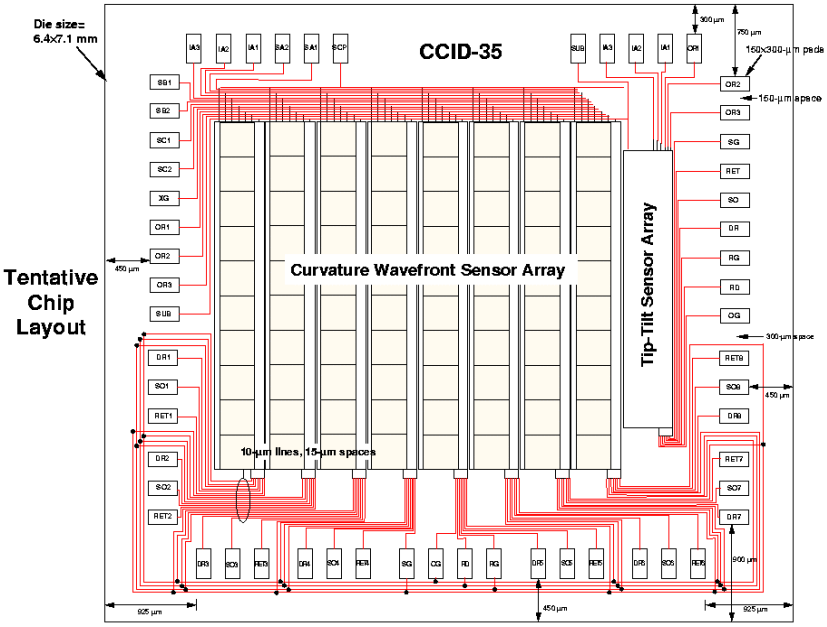

Fig. 2. The curvature-CCD, MIT/LL CCID-35.

3. MODELLING THE SYSTEM

3.1 Properties of the AO-system

The modelled system is the 60-element Multiple Application Concept for Adaptive Optics (MACAO) curvature system that is being developed by ESO. The system has the following properties:

- The telescope is a Unit Telescope of the VLT, which has an 8-meter primary and a 1.12-meter secondary mirror.
- The AO-system uses a 150-mm bimorph mirror, supported in three points, to correct the wavefront deformation in a 100-mm pupil.
- The maximum update rate of the bimorph mirror is 350 Hz.
- The membrane mirror oscillates at a frequency of 2.1 kHz with a minimum absolute focal length of 0.25 m.
- The computational delay in the controller is 500 μs.

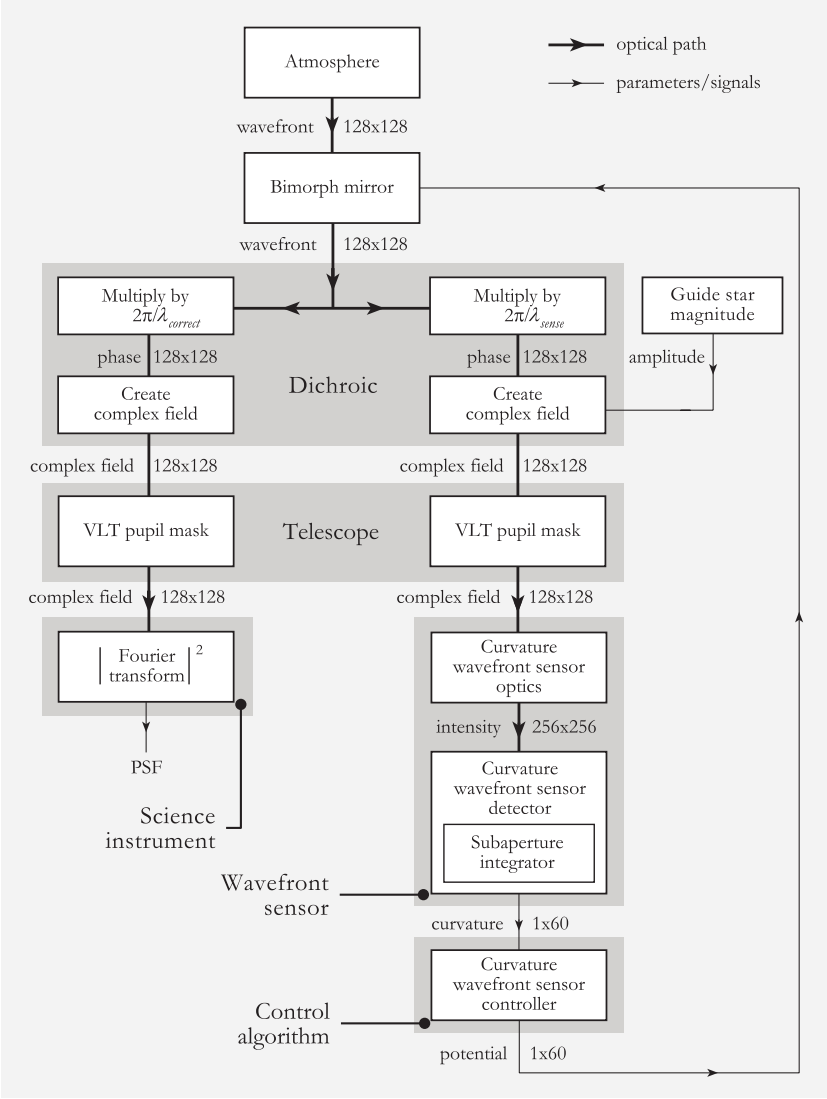

Fig. 3. Structure of the simulation. The optical path is marked with bold lines while other data flows are drawn in thin lines. To the left of these lines, the type of information that the connection passes is indicated, and to the right, the format of the information is specified.

3.2 Properties of the simulation

Fig. 3 shows the structure of the simulation. Some key properties of the simulation and differences to the real system are listed and discussed below.

- ***Spatial sampling of the wavefront***. The wavefront, which measures 8 by 8 meters, is sampled in a 128 by 128 grid, giving a sample distance of 62.5 millimetres.
- ***Temporal sampling of membrane motion***. The fastest changing element in the system is the membrane mirror which oscillates at 2.1 kHz. In the simulation, its motion is sampled 16 times per period, giving a sampling frequency of 33.6 kHz.
- ***Update rate of atmospheric turbulence***. The atmospheric turbulence is updated twice every membrane period, at 4.2 kHz.
- ***Monochromatic wavefront sensor and science camera***. In the simulation, the guide star is assumed to generate light of only two wavelengths: the sensing wavelength λ_{sense}=700 nm and the correction wavelength $\lambda_{correct}$=2.2 μm. This is a significant approximation, as the light from the guide star in reality has a continuous spectrum. However, when calculating the photon flux incident on the detector from a guide star of a certain magnitude, the full spectrum between 400 nm and 1000 nm is considered.
- ***Anisoplanatism***. In the simulation, the Strehl ratio is measured on the point spread function (PSF) of the guide star itself (at 2.2 μm), so anisoplanatism is not taken into account.
- ***Field representation and scintillation***. The electromagnetic field that propagates through the optical path is represented in different ways at different points in the simulation. Since scintillation is neglected in the simulation, the shape of the wavefront, measured in metres, adequately describes the light passing between the atmosphere module and the bimorph mirror. By multiplying the wavefront shape output from the bimorph mirror module by $2\pi/\lambda$, the phase of the light at wavelength λ is obtained. Before the VLT pupil mask is applied, the phase and amplitude are combined to form the complex representation of the light. After the curvature wavefront sensor optics, only the intensity, or photon flux, is used to represent the light.
- ***Telescope pupil mask***. Since the pupil mask of the telescope affects the amplitude of the light, it can be applied only when the representation of the light includes its field amplitude. This means it must be applied to the complex representation of the light and for each wavelength separately. Furthermore, since the spider is only 39 mm wide and the sample distance of the wavefront is 62.5 mm, the spider is neglected and excluded from the pupil mask.
- ***Lenslet array***. In the simulation, the order of the *spatial* integration of light performed by the lenslet array (subaperture integrator) and the *temporal* integration performed by the CWS detector is reversed compared to that of the real system. In this way, the integrated intrafocal and extrafocal can be inspected before their fine structure is lost in the spatial integration of the subaperture integrator.
- ***Exposure time***. The performance measurements of the modelled system are based on two-second exposures. This may seem short in comparison to the real system, where exposures of several minutes are common, but since the task is to compare different configurations of the system, these two-second exposures are sufficient.

3.3 Simulated atmosphere

To simulate the effect that atmospheric turbulence has on the wavefront, a simplified model is used. The following assumptions are made:

- The turbulence is concentrated to a few layers that move in different directions at different speeds.
- The turbulence of each such layer evolves very slowly compared to the speed of the layer, so the layers can be represented by frozen phase screens (this is known as Taylor's hypothesis).
- The telescope is aimed at Zenith, and light is propagated through the atmosphere by simply adding the phase distortions of the different phase screens through a cylinder emanating from the telescope.

The simulated atmosphere is a three-layer model with 0.65" seeing, an r_0 of 15.7 cm, and a τ_0 of 4 ms, all measured at 500 nm. The sky background is magnitude 20.5 per square arcsecond with a one-arcsecond field of view.

3.4 Properties of the detectors

The properties of the compared detectors are listed in Table 1. Note that the quantum efficiency of the CCD is really 20% higher than the APDs, but the additional relay optics used in the prototype system brings this difference down to 10%. In future systems, the relay optics and the consequent loss of light can be avoided by placing the fibres coming from the 60 subapertures of the lenslet array directly in front of the CCD.

Table 1. Specifications of the detectors.

Property	**APDs**	**CCD**
Peak quantum efficiency	70%	80%*
Dark current [electrons/s]	250	0
Read-out noise [electrons RMS]	0	2
Read-out delay [μs]	0	250

* includes light loss in the additional relay optics required for the CCD.

3.5 Loop gains and integration times

Depending on the brightness of the guide star, the loop gain of the controller, the integration time and the frequency at which the shape of the bimorph mirror is updated must be adapted. Table 2 lists these parameters for the simulated guide star magnitudes.

Table 2. Loop gains, integration times and update frequencies used in the simulation.

Guide star magnitude	Integration time [ms]	Update frequency [Hz]	Loop gain
10	2.86	350	0.6
11	2.86	350	0.5
12	2.86	350	0.4
13	2.86	350	0.3
14	4.76	210	0.6
15	4.76	210	0.5
16	6.67	150	0.3
17	14.8	67.7	0.3
18	40.0	25.0	0.3

3.6 Monitoring the simulation

To monitor the progress of the simulation, the monitoring display of Fig. 4 is updated at regular intervals while the simulation is running. The plots in the top row, from left to right, are

- the phase of the uncorrected wavefront.
- the phase correction applied by the bimorph mirror.
- the residual phase aberration of the corrected wavefront.
- the Strehl-plot, which contains two curves – the short-exposure and long-exposure Strehl ratios – as functions of time.

The titles of the first three plots also contain the peak-to-valley value in radians of what each plot displays. The plots in the lower row are the square roots of

- the instantaneous uncorrected PSF.
- the long exposure uncorrected PSF.

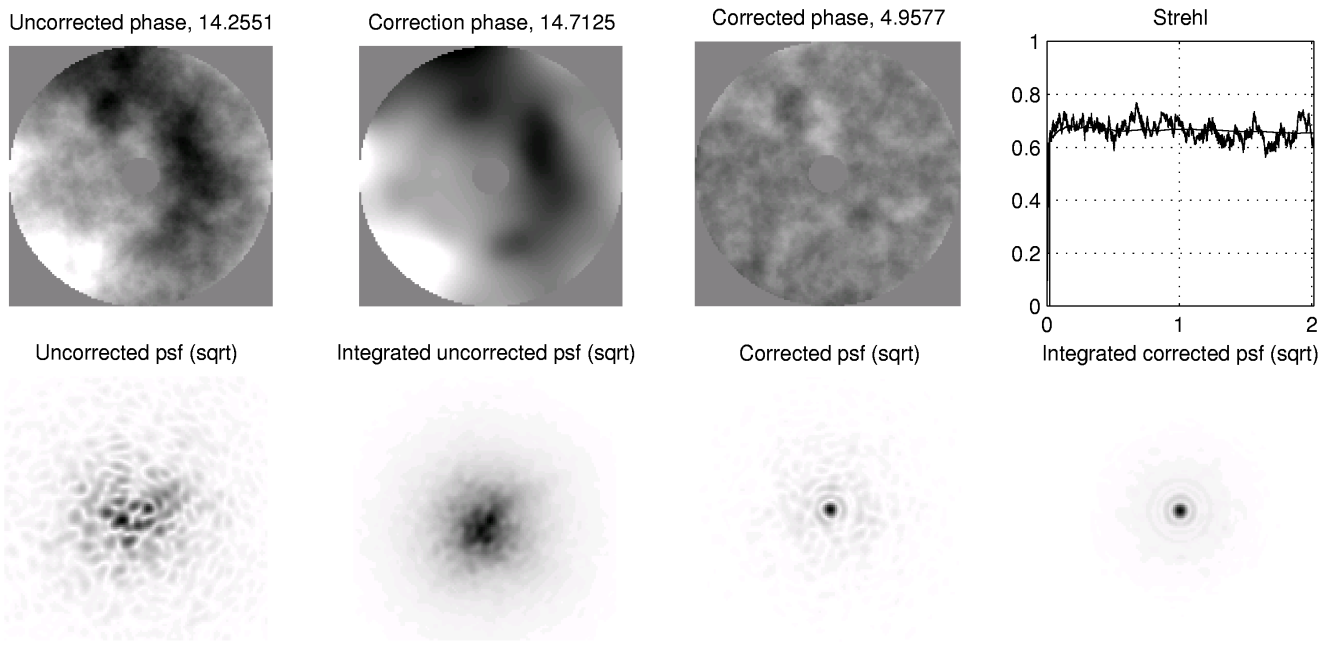

Fig. 4. The monitoring display.

- the instantaneous corrected PSF.
- the long exposure corrected PSF.

4. SIMULATION RESULTS

By measuring the integrated Strehl ratio in K-band achieved by the system for guide stars of magnitude 10 to 18, the curves of Fig. 5 are obtained. As we see, the difference in performance between APDs and the CCD is only significant at magnitude 15 and 16 where the APDs perform better than the CCD by five and two percent Strehl respectively. For all other magnitudes, the difference amounts to less than 0.6 percent Strehl.

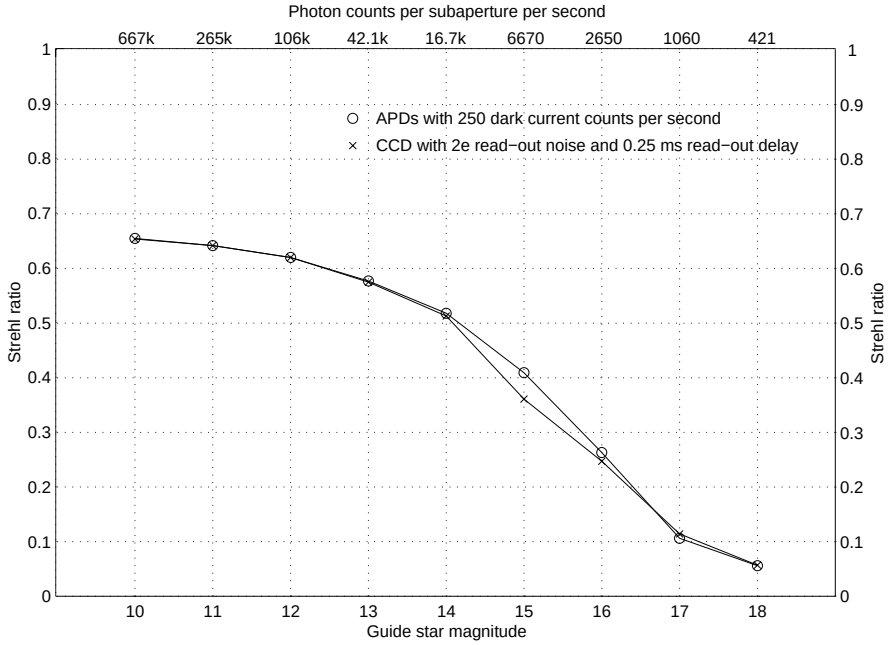

Fig. 5. Strehl ratio in K-band for the different detectors.

5. CONCLUSIONS

There are many factors that must be considered when comparing APDs and CCDs as detectors for the curvature wavefront sensor. The simulation shows that the difference in performance is small. Other relevant factors are:

- ***Reliability***. APDs fail more easily than CCDs. Since there are 60 APDs in a system, the probability of one failing could be significant.
- ***Mechanical complexity***. The neutral density filters and the accompanying filter-wheels required for the APDs increase the mechanical complexity of the system.
- ***Future developments***. In the future, AO-systems with hundreds of subapertures will be built. For such systems, the difference in cost and reliability between the APDs and the CCD will become very significant. With these systems in mind, the development and use of the curvature-CCD seems all the more feasible.
- ***Uncertainty***. Using APDs in curvature wavefront sensors is a proven concept, while the curvature-CCD is a new concept. Results from the ongoing developments at ESO are expected by the end of 2000.

REFERENCES

1. R. Donaldson et al, "Design and current development status of ESO's in-house adaptive optics development: MACAO", submitted to this conference
2. J.W. Beletic et al, "A New CCD Designed for Curvature Wavefront Sensing", *Optical Detectors for Astronomy II*, Kluwer Academic Publishers, 2000
3. J.W. Beletic et al, "FIERA: ESO's New Generation CCD Controller", *Optical Detectors for Astronomy*, Kluwer Academic Publishers, 1998